Theor Chem Acc (2016) 135:50
DOI 10.1007/s00214-016-1805-0

REGULAR ARTICLE

Adsorption mechanisms of lithium oxides (Li_xO_2) on N-doped graphene: a density functional theory study with implications for lithium–air batteries

Ji Hye Lee[1] · Sung Gu Kang[2] · Il Tae Kim[3] · Soonchul Kwon[4] · Inwon Lee[5] · Seung Geol Lee[1]

Received: 8 October 2015 / Accepted: 5 January 2016 / Published online: 15 February 2016

Abstract We utilized density functional theory (DFT) study to understand the adsorption mechanism of lithium oxides (Li_xO_2) onto N-doped graphene during oxygen reduction reaction (ORR) for lithium–air batteries. We systematically proposed two possible ORR pathways and examined various adsorption configurations in each system, including for the O_2 and Li ORR reactants and the LiO_2 and Li_2O_2 ORR products. The doping of the N atom into graphene was calculated to enhance the adsorption of O_2, but to attenuate the adsorption of Li, because of the repulsion between the electron-rich N-doped graphene and the electron-donating Li atom, and the attraction of this N-doped graphene for electronegative O_2. Nevertheless, since the adsorption of Li onto N-doped graphene (−1.001 to −0.503 eV) was still stronger than the adsorption of O_2 (−0.280 to −0.215 eV), Li should bind N-doped graphene first. Moreover, N-doped graphene was calculated to bind LiO_2 (−0.588 eV) more strongly than was pristine graphene (−0.450 eV). Additionally, the Li_2O_2 configuration that yielded the most stable adsorption on N-doped graphene was calculated to yield an adsorption energy of −0.642 eV, which is more favorable than that for pristine graphene (−0.630 eV). Overall, N-doped graphene was found to strengthen the adsorption of lithium oxides (Li_xO_2) and increase charge transfer to substantial levels.

Keywords Lithium–air batteries · N-doped graphene · Oxygen reduction reaction · Lithium oxides · Density functional theory

1 Introduction

Lithium–air batteries have attracted considerable recent attention as a highly promising energy storage system that could replace Li-ion batteries owing to their markedly superior theoretical energy density and low cost [1, 2]. However, the development of lithium–air batteries is still at its initial stage, and there are many technical challenges limiting their practical uses, such as low round-trip efficiency, poor rate capability and low cycle life [1, 2]. These problems mainly result from the sluggish kinetics of the oxygen reduction reaction (ORR) and oxygen evolution reaction (OER) at the cathode.

In an effort to enhance the kinetics at the lithium–air cathode and hence improve the overall performance of the battery, much intensive research has been devoted to the development of high-performance cathode materials [3]. Among the many potential cathode materials, graphene has been considered as one of the most interesting materials because of its unique properties such as large surface area, high electrical conductivity, and good chemical and thermal stability

✉ Seung Geol Lee
seunggeol.lee@pusan.ac.kr

1 Department of Organic Material Science and Engineering, Pusan National University, 2, Busandaehak-ro 63beon gil, Geumjeong-gu, Busan 46241, Republic of Korea

2 Office of Strategic Foresight, Korea Institute of S&T Evaluation and Planning (KISTEP), 68, Mabang-ro, Seocho-gu, Seoul 06775, Republic of Korea

3 Department of Chemical and Biological Engineering, Gachon University, Seongnam-si, Gyeonggi-do 13120, Republic of Korea

4 School of Urban, Architecture and Civil Engineering, Pusan National University, 2, Busandaehak-ro 63beon-gil, Geumjeong-gu, Busan 46241, Republic of Korea

5 Global Core Research Center for Ships and Offshore Plants (GCRC-SOP), Pusan National University, Busandaehak-ro 63beon-gil, Geumjeong-gu, Busan 46241, Republic of Korea

[4]. In addition, graphene can be easily tailored by diverse modification methods. Hence, further developments involving modifying the surface of graphene have been made in order to promote the electro-catalytic activity of the graphene electrode during the ORR and thus improve the specific capacity and cycling performance of the battery [5–25].

Among the various potential surface modifications, doping heteroatoms into graphene has attracted substantial interest due to its effectiveness at tailoring the electronic and chemical properties and enhancing catalytic activity [11, 12]. The N atom in particular is one of the most promising candidates for doping because its atomic size is closest to that of the C atom, and hence can be relatively easily made to substitute for a C atom in the lattice of hexagonal rings of graphene. Therefore, N-doped graphene has been more easily synthesized than have other types of doped graphene, and its synthesis has recently been actively carried out using several different methods, such as chemical vapor deposition (CVD) [26], thermal treatment [27, 28] and plasma treatment [29]. Furthermore, N-doped graphene has been found to be an even more excellent catalyst for the ORR than have noble metal (Pt, Au) and transition metal oxides (MnO_2, Fe_2O_3, Co_3O_4) due to its availability and comparatively low price and hence suitability for large-scale production and commercialization [13–22]. However, the catalytic activity of N-doped graphene is still a subject of debate, and the molecular-scale mechanism by which Li_xO_2 lithium oxides adsorb on N-doped graphene during the ORR has not yet been fully clarified.

Herein, we used density functional theory (DFT) calculations to gain an understanding of the mechanism of the adsorption of Li_xO_2 lithium oxides on N-doped graphene. This mechanism was investigated by calculating the adsorption energies of ORR reactants O_2 and Li and of ORR products LiO_2 and Li_2O_2 on N-doped graphene and analyzing the accompanying electronic structures and properties, such as the band structure, density of states (DOS), derived electrostatic and chemical (DDEC) charge distribution, and electronic charge density distribution.

2 Computational methods

All calculations were performed within the DFT framework as implemented in the Vienna ab initio simulation package (VASP) [30, 31] to solve the Kohn–Sham equations with a plane-wave basis set, with a kinetic energy cutoff of 500 eV. The projector augmented wave (PAW) potential [32] was applied to describe core electrons. The spin-polarized generalized gradient (GGA) approximation with the Perdew–Burke–Ernzerhof (PBE) functional [33, 34] was employed to treat the exchange–correlation energy of interacting electrons. The GGA–PBE functional has been widely used to investigate carbon-based materials [35–42]. The 4 × 4 supercell model of graphene, which was set to 9.84 Å × 9.84 Å × 15 Å, was used. We selected the N-substituted graphene due to the lowest formation energy compared with other N-doped defect graphene including pyridinic or pyrrolic configuration [43]. The calculations were performed within the periodic boundary conditions, with 15 Å of vacuum space included, large enough to avoid direct interactions between the original structure and its periodically repeated image along the c-axis. The Brillouin zone was sampled with 5 × 5 × 1 k-point meshes centered at the gamma point using the Monkhorst–Pack scheme. Atomic positions were fully relaxed until the forces on each atom were smaller than 0.01 eV/Å and the total energies were converged within 10^{-6} eV. For all geometrical optimizations, a dipole correction was applied to compensate for the dipole interactions along the c-axis direction. The DFT-D3 correction of the Grimme scheme was incorporated with the PBE functional to account for the van der Waals interactions [44]. The adsorption energy of each system ($\Delta E_{\text{adsorption}}$) was calculated by using the definition.

$$\Delta E_{\text{adsorption}} = E_{\text{total}} - (E_{n-\text{graphene}} + E_{\text{adsorbate}}) \quad (1)$$

where E_{total} is the total energy of the system, $E_{\text{n-graphene}}$ is the energy of the N-doped graphene and $E_{\text{adsorbate}}$ is the energy of the adsorbate species in a vacuum, respectively. Please note that, according to this definition, a negative value of the adsorption energy indicates that adsorption is favorable, whereas a positive value indicates that it is unfavorable. To evaluate the quantitative charge distributions between the adsorbate species and graphene surface, the density-derived electrostatic and chemical (DDEC) method [45] was performed. To study the diffusion of Li atom on N-doped graphene, we used the climbing image nudge elastic band (CI-NEB) method.

3 Results and discussion

3.1 Adsorption of O_2 on N-doped graphene

In order to understand the adsorption mechanism of Li_xO_2 lithium oxides, which are ORR products, we considered two possible pathways to produce these oxides: $O_2 \rightarrow LiO_2 \rightarrow Li_2O_2$ and $Li \rightarrow LiO_2 \rightarrow Li_2O_2$. The former denotes an ORR pathway in which an O_2 molecule initially adsorbs onto N-doped graphene and then Li atoms adsorb onto the N-doped graphene and adsorbed O_2, whereas the latter indicates the initial anchoring of one Li atom on N-doped graphene that are then bound by an O_2 molecule and a second Li atom. We aimed to predict which of the two pathways predominate by investigating the numerous possible adsorption structures.

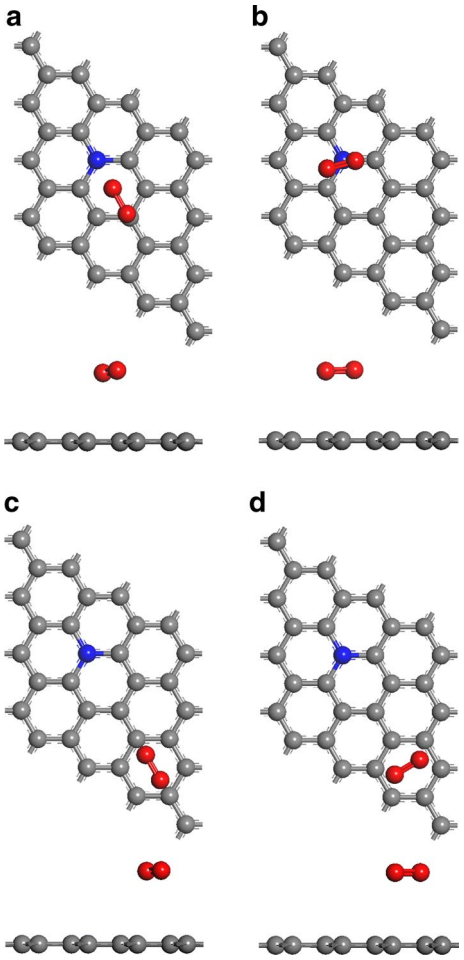

Fig. 1 Optimized structures of the various configurations of O_2 adsorbed on N-doped graphene: **a** *top* and *side views* of O_2_A, **b** *top* and *side views* of O_2_B, **c** *top* and *side views* of O_2_C, **d** *top* and *side views* of O_2_D. The *gray*, *red* and *blue colors* denote carbon, oxygen and nitrogen, respectively

First, we considered the various possible adsorption sites of the O_2 molecule on N-doped graphene, as shown in Fig. 1. We considered the adsorption sites in which O_2 spans a hexagonal ring that contains a doped N atom (configurations "O_2_A" and "O_2_B") and in which O_2 similarly spans an all-carbon hexagonal ring far from an N atom (configurations "O_2_C" and "O_2_D"). In configuration O_2_A, the O_2 molecule was initially made to form a bridge "over" the N-containing ring from the nitrogen atom to the opposing (para) carbon atom, whereas in configuration O_2_B it was made to form a bridge between the midpoints of opposite C–C bonds. Similarly, O_2 was started off bridging para-related carbons of the all-carbon ring in configuration O_2_C and opposite C–C bonds of the all-carbon ring in configuration O_2_D. The considered sites were: (1) site O_2_1A, in which O_2 lays across the midpoint of the C–C bond; (2) site O_2_1B, in which O_2 lays across two opposing carbon atoms; (3) site O_2_1C, in which the O_2 lays across two adjacent carbon atoms; and (4) site O_2_1D, in which the O_2 lays above the center of a hexagon ring. The adsorption energies, DDEC charge distributions, distance from the graphene to the center of mass of O_2 and the bond length of O_2 at various adsorption sites are given in Table 1.

The adsorption energies, charge distributions through DDEC charge analysis, vertical distance from the N-doped graphene to the center of mass of O_2 and the bond length of O_2 at the various adsorption configurations are given in Table 1. The adsorption energies for O_2 adsorbed on the hexagonal ring containing an N atom in configurations O_2_A and O_2_B were calculated using DFT to be stronger than those for O_2 adsorbed on the all-carbon ring in configurations O_2_C and O_2_D. The adsorption energies of the O_2 molecule on N-doped graphene were in the range of −0.280 to −0.215 eV and hence stronger than the adsorption energies of −0.111 to −0.089 eV on pristine graphene in our previous study [46]. The distance between the O_2 molecule and N-doped graphene (3.015 and 3.173 Å for the two configurations) was shorter than the distance between the O_2 molecule and pristine graphene (3.204 and 3.284 Å). In addition, due to the higher electronegativity of O than C and N, substantial charge (−0.255 to −0.169e) was transferred from N-doped graphene to O_2, compared with pristine graphene (−0.036e) [46]. Therefore, these results indicated that N doping enhanced the interaction between the O_2 molecule and graphene, but O_2 was still weakly physisorbed onto N-doped graphene.

Table 1 Adsorption energy, DDEC charge distribution, vertical distance from N-doped graphene to O_2 and bond length of O_2 for various adsorption configurations in the O_2-adsorbed N-doped graphene

Adsorption configuration	Adsorption energy(eV)	Graphene–O_2 distance (Å)	O–O bond length (Å)	Charges (*e*)	
				O_2	Graphene
O_2_A	−0.262	3.032	1.258	−0.188	0.188
O_2_B	−0.280	3.015	1.260	−0.255	0.255
O_2_C	−0.215	3.173	1.255	−0.169	0.169
O_2_D	−0.218	3.116	1.255	−0.170	0.170

3.2 Adsorption of Li on N-doped graphene

Next, we placed a Li atom on N-doped graphene in various possible adsorption configurations. As shown in Fig. 2, three high-symmetry adsorption sites were considered: (1) the site above the C atom nearest the N atom (configuration Li_A); (2) the site above the center of the hexagonal ring containing an N atom (configuration Li_B); and (3) the site above the center of the all-carbon ring farthest from the N atom (configuration Li_C). The adsorption energies of the Li atom onto N-doped graphene varied from −1.001 to −0.503 eV, as shown in Table 2. The site above the center of the all-carbon hexagonal ring farthest from the N atom (configuration Li_C) was the most favorable position for the adsorption of Li, with an adsorption energy of −1.001 eV and a distance of 1.683 Å, indicative of a strong Coulombic interaction. Note that increasing the distance between the adsorbed Li atom and the N atom resulted in stronger interactions between Li and graphene. However, in contrast to the adsorption energies of a Li atom (−1.079 to −0.768 eV) and the amount of transferred charge (−0.917 to −0.910 e) on pristine graphene [46], the adsorption energies and the amounts of transferred charge on N-doped graphene were decreased. These results may be explained by the Li atom having a tendency to readily lose an electron in order to attain a stable complete-shell electron configuration, whereas electron-rich N-doped graphene tends not to accept more electrons [47], resulting in the N atom on N-doped graphene and the Li atom repelling each other. However, the Li atom in our calculations still adsorbed (−1.001 to −0.503 eV) more strongly onto N-doped graphene than did the O_2 molecule (−0.280 to −0.215 eV), and the vertical distance between the Li atom and N-doped graphene (1.683–1.982 Å) was shorter than this distance between the O_2 molecule and N-doped graphene (3.015–3.173 Å). Moreover, the charge transferred from the Li atom to N-doped graphene (−0.895 to −0.868 e) was larger than that transferred from the O_2 molecule (−0.255 to −0.169 e). Thus, we predict that a Li atom would tend to adsorb onto N-doped graphene before an O_2 molecule would do so, and that the ORR mechanism would therefore preferentially follow the Li → LiO_2 → Li_2O_2 pathway. Because Li atom was preferentially adsorbed on N-doped graphene, it is important to figure out the diffusion of Li atom on N-doped graphene. As shown in Fig. 3, we calculated the diffusion of Li atom between site Li_B and site Li_C on N-doped graphene. The energy barrier for the diffusion of Li atom from site Li_B to site Li_C was ~ 0.10 eV (~ 0.43 eV for the opposite direction). It means that Li atom can be easily diffused toward the region which is far from the hexagonal ring containing N atom.

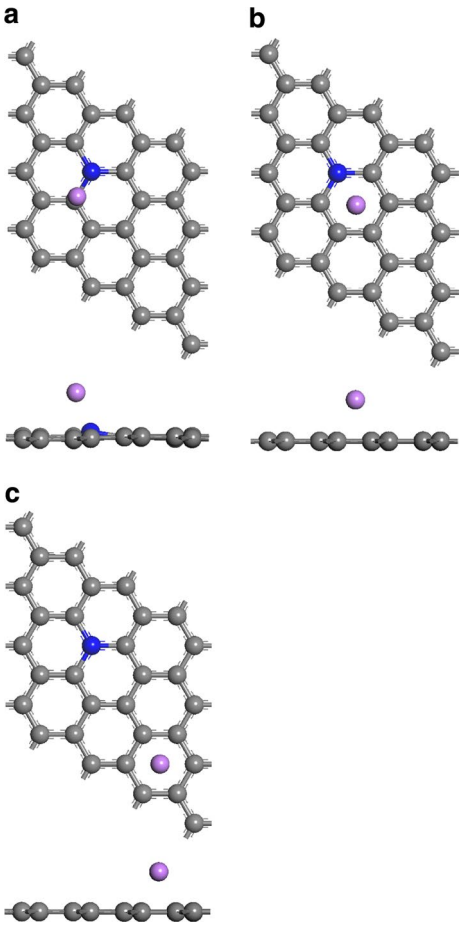

Fig. 2 Optimized structures of the various configurations of Li adsorbed on N-doped graphene: **a** *top* and *side views* of Li_A; **b** *top* and *side views* of Li_B; **c** *top* and *side views* of Li_C. The *gray*, *purple* and *blue colors* denote carbon, lithium and nitrogen, respectively

3.3 Adsorption of Li_xO_2 on N-doped graphene

We next simulated the adsorption of LiO_2 on N-doped graphene with a configuration in which the Li atom of LiO_2 was initially positioned on the center of the hexagonal ring containing the N atom. Geometry optimization resulted in this Li atom moving farther away from the N atom, as shown in Fig. 4a. The distance between LiO_2 and N-doped graphene was calculated to be 2.438 Å, and the corresponding adsorption energy was calculated to be −0.588 eV (Table 3), which is stronger than that for pristine graphene (−0.450 eV) [46].

We also investigated the structures consisting of Li_2O_2 adsorbed onto N-doped graphene. There are two possible adsorption sites based on the adsorption configuration of O_2 onto N-doped mentioned above. As shown in Fig. 4b, c, the considered configurations were as follows: (1) configuration Li_2O_2_A, in which the two Li atoms of the Li_2O_2 molecule were positioned above the midpoints of

Table 2 Adsorption energy, DDEC charge distribution and vertical distance from N-doped graphene to Li for various adsorption configurations in the Li-adsorbed N-doped graphene

Adsorption configuration	Adsorption energy (eV)	Graphene–Li distance (Å)	Charges (*e*)	
			Li	Graphene
Li_A	−0.503	1.982	0.868	−0.868
Li_B	−0.675	1.718	0.895	−0.895
Li_C	−1.001	1.683	0.892	−0.892

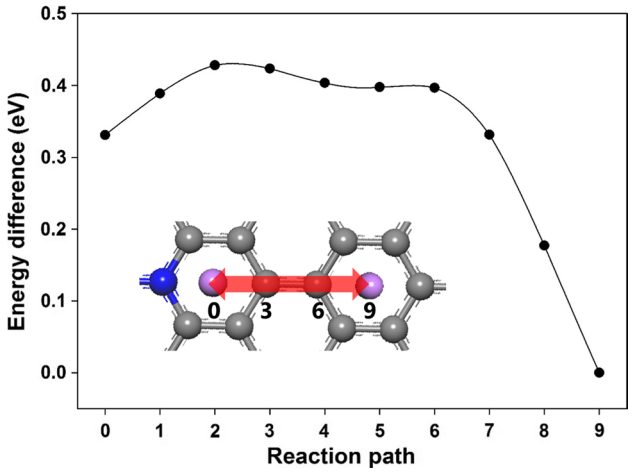

Fig. 3 Energy profile for the diffusion of Li atom along the pathway between site Li_B and site Li_C on N-doped graphene

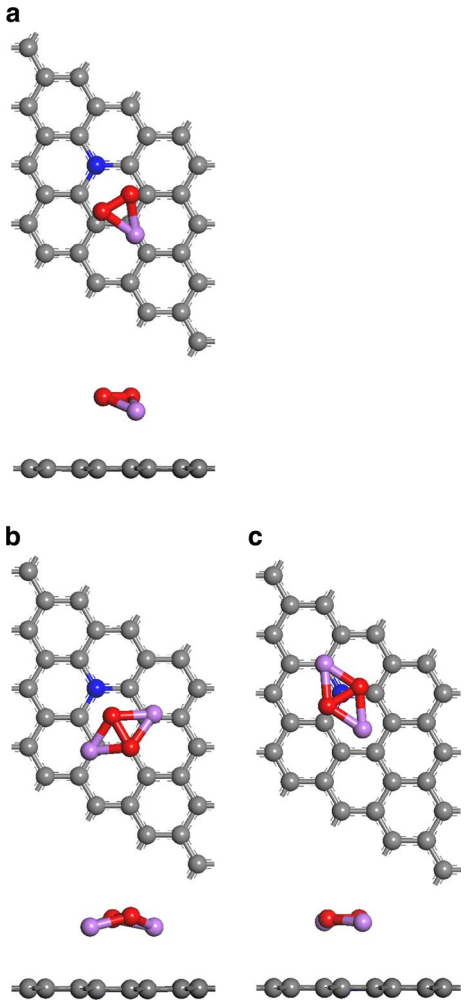

Fig. 4 Optimized structures of the various configurations of Li_xO_2 adsorbed on N-doped graphene: **a** *top* and *side views* of LiO_2_A, **b** *top* and *side views* of Li_2O_2_A, **c** *top* and *side views* of Li_2O_2_B. The *gray*, *red*, *purple* and *blue colors* denote carbon, oxygen, lithium and nitrogen, respectively

opposite C–C bonds and the two O atoms in Li_2O_2 were, respectively, positioned above the N atom and the para C atom; and (2) configuration Li_2O_2_B, in which the Li_2O_2 of Li_2O_2_A was essentially rotated by 90°. Li_2O_2 in both configurations Li_2O_2_A and Li_2O_2_B experienced substantial structural deformations upon optimization; their structures became bent in response to a close approach of the Li_2O_2 of Li atoms to the graphene. Configuration Li_2O_2_A was calculated to have the more favorable adsorption, with an adsorption energy of −0.642 eV, which is stronger than those on pristine graphene (−0.630 to −0.611 eV) [46]. Li_2O_2_A also displayed the shorter distance between Li_2O_2 and N-doped graphene (2.607 Å) and was accompanied by substantial charge transfer (|0.241*e*|).

3.4 Analysis of the other electronic properties

We also investigated the electronic properties of all the systems in order to gain further insight into their adsorption behaviors. Figure 5 shows the band structure of graphene, N-doped graphene, O_2-adsorbed N-doped graphene, Li-adsorbed N-doped graphene, LiO_2-adsorbed N-doped graphene and Li_2O_2-adsorbed N-doped graphene systems. We chose the most stable configurations for each system to analyze the electronic properties. The band structure of pristine graphene featured Dirac points at the Fermi level, in which the valence and conduction bands coincide, and displays metallic characteristics with a zero band gap. Because the N atom, with its five valence electrons, has one more valence electron than does the C atom, the doping of the N atom into graphene makes it a more electron-rich system. Hence, the band structures of N-doped graphene showed energy bands that were shifted down to the Fermi level, as shown in Fig. 5b. In addition,

Table 3 Adsorption energy, DDEC charge distribution and vertical distance from N-doped graphene to the Li atom of Li_xO_2 for various adsorption configurations in the Li_xO_2-adsorbed N-doped graphene

Adsorption configuration	Adsorption energy (eV)	Graphene–Li distance (Å)	Charges (*e*)		
			Li	O_2	Graphene
LiO_2_A	−0.588	2.438	0.832	−0.832	0
Li_2O_2_A	−0.642	2.607	1.826	−1.585	−0.241
Li_2O_2_B	−0.604	2.758	1.854	−1.682	−0.172

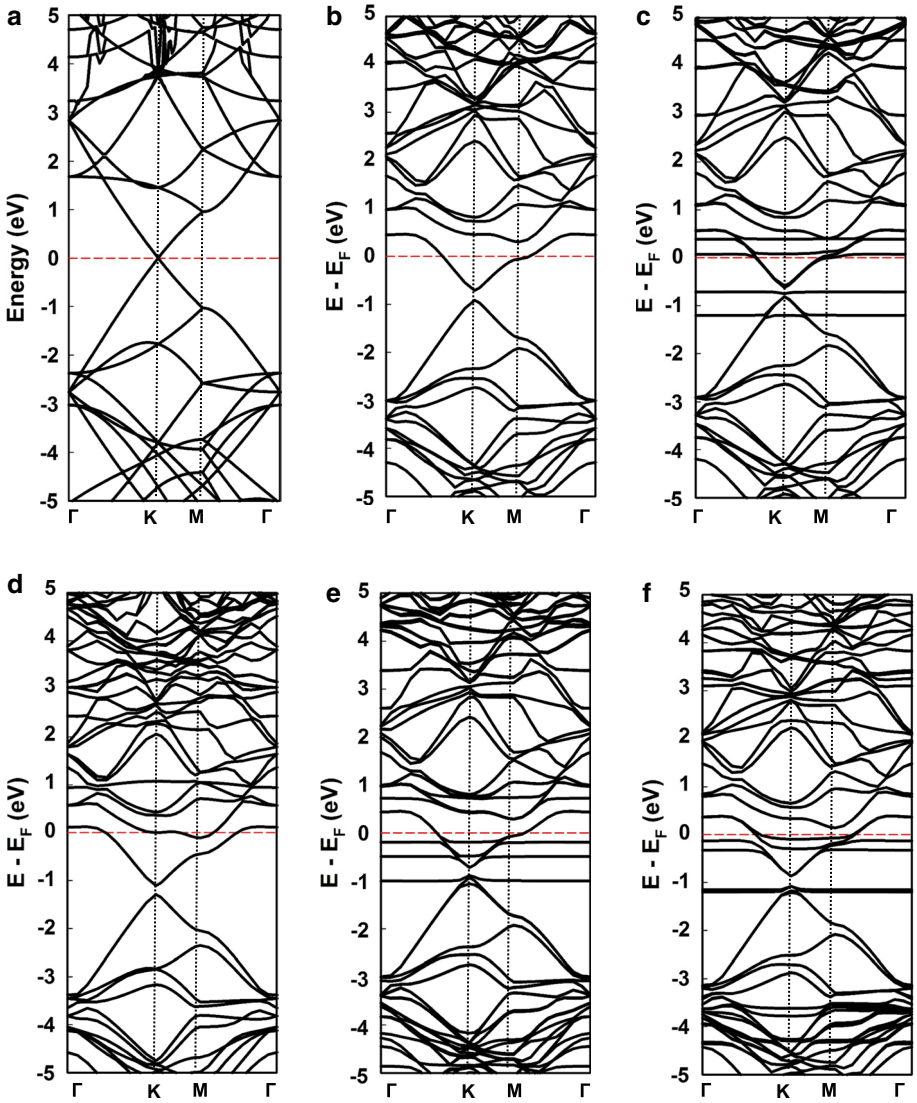

Fig. 5 Band structures of **a** graphene, **b** N-doped graphene, **c** N-doped graphene/O_2, **d** N-doped graphene/Li, **e** N-doped graphene/LiO_2 and **f** N-doped graphene/Li_2O_2

we found that the Dirac point, which is a specific property of graphene, became blurred due to the breaking of the symmetry of the graphene sub-lattices that resulted from the inclusion of the N atom [48]. In the N-doped graphene/O_2 system (Fig. 5c), the energy bands were slightly shifted up in comparison with the pristine N-doped graphene system owing to the hybridization between O_2 and N-doped graphene orbitals. As compared to the case of the pristine N-doped graphene system, the N-doped graphene/Li system (Fig. 5d) showed that the energy bands were downshifted because of the electron injection from the Li atom to N-doped graphene. In the N-doped graphene/LiO_2 system (Fig. 5e), the slightly more downshifted energy bands, compared to those of the N-doped graphene system, resulted from the hybridization between Li, O_2 and N-doped graphene. In the N-doped graphene/Li_2O_2 system (Fig. 5f), we found more band shifts than for the N-doped graphene/LiO_2 system because electrons from the two Li atoms of Li_2O_2 were injected into N-doped graphene.

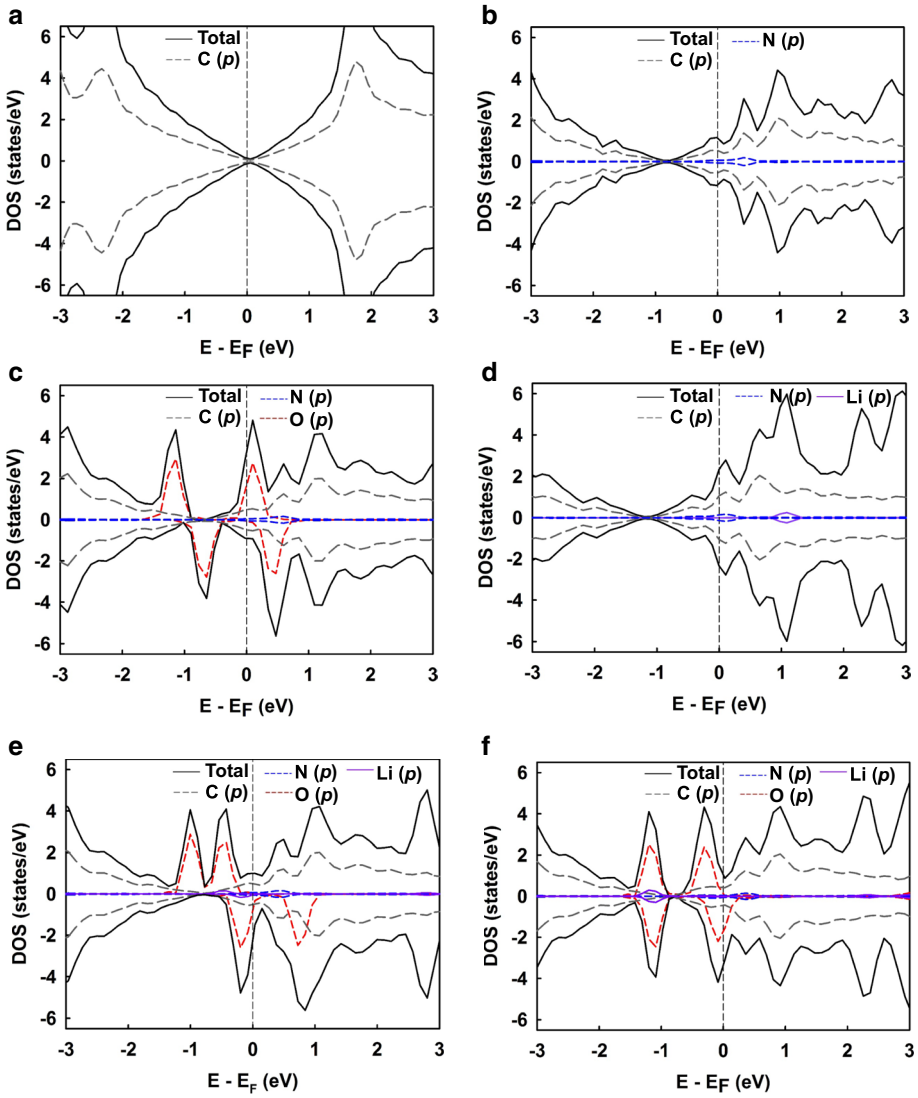

Fig. 6 Density of states (DOS) and local density of states (LDOS) of **a** graphene, **b** N-doped graphene, **c** N-doped graphene/O_2, **d** N-doped graphene/Li, **e** N-doped graphene/LiO_2 and **f** N-doped graphene/Li_2O_2

To gain a deep understanding of the electronic structures in each system, we examined the density of states (DOS) and local density of states (LDOS), as shown in Fig. 6. The DOS of pristine graphene and N-doped graphene are shown in Fig. 6a, b, respectively. The DOS of pristine graphene featured a zero DOS at the Fermi level, and that of N-doped graphene was downshifted to below the Fermi level due to its electron-rich character resulting from the doping of the N atom. In the N-doped graphene/O_2 system (Fig. 6c), the adsorption of O_2 on N-doped graphene introduced the appearance of spin polarization, which was caused by a new spin-up O *p* peak around the Fermi level. In the N-doped graphene/Li system (Fig. 6d), the overall DOS was downshifted, as compared with the DOS of N-doped graphene system, and the DOS peak around the Fermi level was increased. The DOS of the Li *s* orbital was found to partially contribute to the total DOS according to the LDOS analysis. In the case of the N-doped graphene/LiO_2 and N-doped graphene/Li_2O_2 systems (Fig. 6e, f), the total DOS were observed to be shifted down and the hybridization of the O *p*, Li *s*, C *p* and N *p* orbitals contributed to the introduction of spin polarization of the total DOS. Furthermore, we calculated the charge density difference of lithium oxides (LiO_2 and Li_2O_2) adsorbed on the N-doped graphene system, $\Delta\rho$, which was defined as follows.

$$\Delta\rho = \rho_{\text{total}} - (\rho_{n-\text{graphene}} + \rho_{\text{adsorbate}}) \quad (2)$$

where ρ_{total}, $\rho_{n\ -\ graphene}$ and $\rho_{adsorbate}$ denoted the charge distributions of the total system, of an N-doped graphene surface and of an isolated adsorbate species in vacuum, respectively. Figure 7a, b shows the charge density difference of lithium oxides (LiO_2 and Li_2O_2) adsorbed onto N-doped graphene. The yellow-colored region represents charge accumulation, and the blue-colored region represents charge depletion. The calculations for both systems

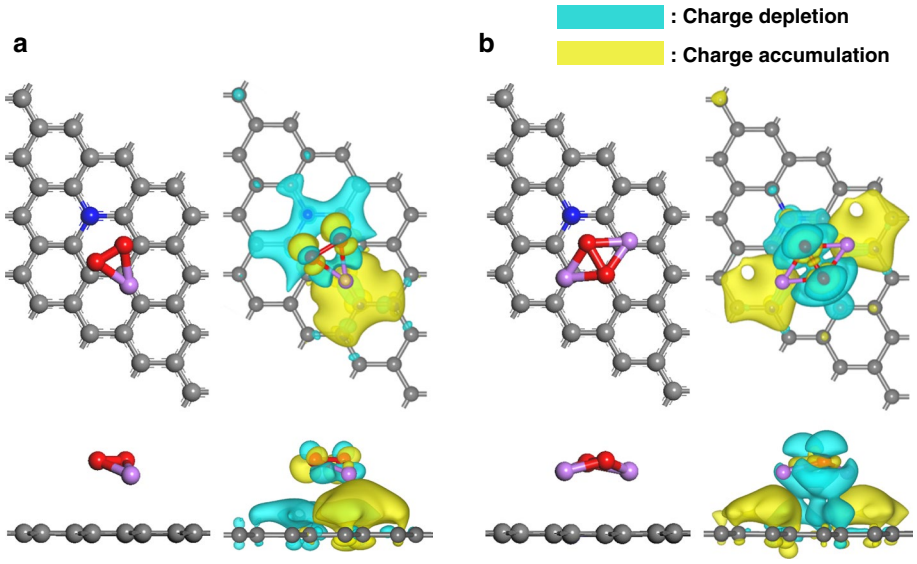

Fig. 7 Plots of charge density difference **a** for N-doped graphene/LiO_2 and **b** for N-doped graphene/Li_2O_2

found a net gain of most charges between the Li atom of the lithium oxides and N-doped graphene. In addition, the gain of electron charge remained in the regions between the oxygen atoms of lithium oxides because of the strong electronegativity of the O atom. These results showed that the most charge was transferred from the Li of lithium oxides (Li_xO_2) to N-doped graphene due to the tendency of Li to easily lose electrons, and therefore a substantial interaction between N-doped graphene and lithium oxides in the intermediate region was observed. Moreover, in our calculations, Li_2O_2 adsorbed more strongly onto N-doped graphene than did LiO_2 because the Li_2O_2-adsorbed N-doped system had a wider charge accumulation region than did the LiO_2-adsorbed N-doped system.

4 Conclusions

We performed DFT calculations to elucidate the adsorption mechanisms of lithium oxides (Li_xO_2) onto N-doped graphene. We considered $O_2 \rightarrow LiO_2 \rightarrow Li_2O_2$ and $Li \rightarrow LiO_2 \rightarrow Li_2O_2$ ORR pathways and modeled adsorption properties of the ORR reactants O_2 and Li and of the ORR products LiO_2 and Li_2O_2. Our results showed that in the case of N-doped graphene, the adsorption energies of the O_2 molecule ranged from −0.280 to −0.215 eV, which were stronger than the adsorption energies (−0.111 to −0.089 eV) on pristine graphene. Moreover, the amount of charge transferred between the adsorbed O_2 molecule and N-doped graphene was calculated to be greater than that for O_2 adsorbed on pristine graphene, and the vertical distance between O_2 and N-doped graphene was less than that between O_2 and pristine graphene. Meanwhile, the N-doped graphene achieved in our calculations lowers adsorption energies of Li (−1.001 to −0.503 eV) with less charge transfer (−0.895 to −0.868 e) than did the pristine graphene (−1.079 to −0.768 eV). In addition, the calculated adsorption energies clearly tended to increase as the O_2 molecule was moved closer to the substituted N atom, and as the Li atom was moved away from the N atom, results that can be explained by the doping of the N atom making graphene an electron-rich system. Hence, the electron-donating Li atom preferred to be adsorbed onto a site of graphene far away from the electron-rich N-substituted hexagonal ring, whereas electronegative O_2 favored this ring as the adsorption site. However, because the adsorption of Li onto graphene was still found to be stronger than the adsorption of O_2 onto graphene, we conclude that the Li atom may be adsorbed by graphene before O_2 is adsorbed, and therefore the ORR may preferentially follow the $Li \rightarrow LiO_2 \rightarrow Li_2O_2$ pathway. For all of the LiO_2 and Li_2O_2 adsorption configurations, the N-doped graphene bound LiO_2 and Li_2O_2 more strongly than did pristine graphene in our calculations. The band energies and DOS in the N-doped graphene/LiO_2 and N-doped graphene/Li_2O_2 systems were shifted down compared to those of the bare N-doped graphene system due to electron injection of the Li atom of lithium oxides. In addition, according to the electronic charge density distribution analysis, much of the transferred charges were accumulated in the region between the Li atoms of the lithium oxides and the N-doped graphene. These results indicate an enhancement of the adsorption of lithium oxides (Li_xO_2) with significant charge transfer by N doping of graphene.

Acknowledgments This research was supported by Basic Science Research Program through the National Research Foundation of Korea (NRF) funded by the Ministry of Science, ICT and Future

Planning (2014R1A1A1004096 and 2015R1C1A1A02036472). This work was financially supported by the National Research Foundation of Korea (NRF) grant funded by the Korea government (MSIP) through GCRC-SOP (No. 2011-0030013).

References

1. Girishkumar G, McCloskey B, Luntz AC, Swanson S, Wilcke W (2010) J Phys Chem Lett 1:2193
2. Kraytsberg A, Ein-Eli Y (2011) J Power Sources 196:886
3. Franco AA, Xue KH (2013) Ecs J Solid State Sci Technol 2:M3084
4. Allen MJ, Tung VC, Kaner RB (2010) Chem Rev 110:132
5. Xiao J, Mei DH, Li XL, Xu W, Wang DY, Graff GL, Bennett WD, Nie ZM, Saraf LV, Aksay IA, Liu J, Zhang JG (2011) Nano Lett 11:5071
6. Yoo E, Zhou HS (2011) ACS Nano 5:3020
7. Wang ZL, Xu D, Xu JJ, Zhang LL, Zhang XB (2012) Adv Funct Mater 22:3699
8. Yoo E, Zhou HS (2014) RSC Adv 4:13119
9. Ren XD, Zhu JZ, Du FM, Liu JJ, Zhang WQ (2014) J Phys Chem C 118:22412
10. Wang S, Dong SM, Wang J, Zhang LX, Han PX, Zhang CJ, Wang XG, Zhang KJ, Lan ZG, Cui GL (2012) J Mater Chem 22:21051
11. Li YL, Wang JJ, Li XF, Geng DS, Banis MN, Li RY, Sun XL (2012) Electrochem Commun 18:12
12. Lin ZY, Waller GH, Liu Y, Liu ML, Wong CP (2013) Carbon 53:130
13. Li Q, Cao RG, Cho J, Wu G (2014) PCCP 16:13568
14. Debart A, Bao J, Armstrong G, Bruce PG (2007) J Power Sources 174:1177
15. Lu YC, Xu ZC, Gasteiger HA, Chen S, Hamad-Schifferli K, Shao-Horn Y (2010) J Am Chem Soc 132:12170
16. Lu YC, Gasteiger HA, Parent MC, Chiloyan V, Shao-Horn Y (2010) Electrochem Solid State Lett 13:A69
17. Choi R, Jung J, Kim G, Song K, Kim YI, Jung SC, Han YK, Song H, Kang YM (2014) Energy Environ Sci 7:1362
18. Su DW, Kim HS, Kim WS, Wang GX (2013) J Power Sources 244:488
19. Wang YG, Zhou HS (2010) J Power Sources 195:358
20. Cheng H, Scott K (2010) J Power Sources 195:1370
21. Debart A, Paterson AJ, Bao J, Bruce PG (2008) Angewandte Chemie-Int Edn 47:4521
22. Minowa H, Hayashi M, Hayashi K, Kobayashi R, Takahashi K (2013) J Power Sources 244:17
23. Chen Y, Zhang Q, Zhang Z, Zhou X, Zhong Y, Yang M, Xie Z, Wei J, Zhou Z (2015) J Mater Chem A 3:17874
24. Zhang Z, Bao J, He C, Chen Y, Wei J, Zhou Z (2014) Adv Funct Mater 24:6826
25. Jing Y, Zhou Z (2015) ACS Catal 5:4309
26. Wei DC, Liu YQ, Wang Y, Zhang HL, Huang LP, Yu G (2009) Nano Lett 9:1752
27. Guo BD, Liu QA, Chen ED, Zhu HW, Fang LA, Gong JR (2010) Nano Lett 10:4975
28. Sheng ZH, Shao L, Chen JJ, Bao WJ, Wang FB, Xia XH (2011) ACS Nano 5:4350
29. Lin YC, Lin CY, Chiu PW (2010) Appl Phys Lett 96:133110
30. Kresse G, Furthmuller J (1996) Phys Rev B 54:11169
31. Kresse G, Furthmuller J (1996) Comp Mater Sci 6:15
32. Blochl PE (1994) Phys Rev B 50:17953
33. Perdew JP, Burke K, Ernzerhof M (1996) Phys Rev Lett 77:3865
34. Perdew JP, Burke K, Wang Y (1996) Phys Rev B 54:16533
35. Park H, Noh SH, Lee JH, Lee WJ, Jaung JY, Lee SG, Han TH (2015) Sci Rep 5:14163
36. Koh W, Lee JH, Lee SG, Choi JI, Jang SS (2015) RSC Adv 5:32819
37. Moon HS, Lee JH, Kwon S, Kim IT, Lee SG (2015) Carbon Lett 16:116
38. Koh W, Choi JI, Lee SG, Lee WR, Jang SS (2011) Carbon 49:286
39. Koh W, Choi JI, Jeong E, Lee SG, Jang SS (2014) Curr Appl Phys 14:1748
40. Kwon S, Lee SG (2015) Carbon Lett 16:198
41. Koh W, Choi JI, Donaher K, Lee SG, Jang SS (2011) ACS Appl Mater Inter 3:1186
42. Koh W, Moon HS, Lee SG, Choi JI, Jang SS (2015) ChemPhysChem 16:789
43. Yu Y-X (2013) PCCP 15:16819
44. Grimme S, Antony J, Ehrlich S, Krieg H (2010) J Chem Phys 132:154104
45. Manz TA, Sholl DS (2010) J Chem Theory Comput 6:2455
46. Lee JH, Kang SG, Moon HS, Park H, Kim IT, Lee SG (2015) Appl Surf Sci 351:193
47. Wu DH, Li YF, Zhou Z (2011) Theor Chem Acc 130:209
48. Rani P, Jindal VK (2013) RSC Adv 3:802